Investigation of Layered Intergrowth $Li_xM_yMn_{1-y}O_{2+z}$ (M = Ni, Co, Al) Compounds as Positive Electrodes for Li-ion Batteries

M. Dollé,* J. Hollingsworth,* T. J. Richardson,† and M. M. Doeff*

**Materials Sciences Division and*
†Environmental Energy Technologies Division
Lawrence Berkeley National Laboratory
University of California
Berkeley, CA 94720, USA

Abstract

Layered substituted lithium manganese oxides suitable for use as lithium ion battery electrodes may be prepared from the corresponding sodium manganese metal oxide compounds by ion-exchange. Stacking arrangements (O2, O3, or O2/O3 intergrowths) in the lithiated materials are dependent upon the Na/transition metal ratio in the sodium-containing precursors, the degree of substitution, and the identity of the substituting metal. O3 layered materials deliver up to 200 mAh/g at moderate current densities in lithium cell configurations, but convert rapidly to spinels upon cell cycling, while O2 compounds are more stable but deliver less capacity. Intergrowths show intermediate behavior, with higher capacities than pure O2 materials and better phase stability than O3 compounds. Some intergrowth structures do not appear to convert to spinel during normal cycling, suggesting it may be possible to tailor high energy density, phase stable layered manganese oxide electrodes for lithium batteries.

Keywords: Lithium batteries, layered manganese oxides, intergrowths

Introduction

Electric vehicles require high energy density batteries that are low-cost and robust. Li-ion batteries are presently being considered for this application but performance needs to be improved, and the expensive $LiCoO_2$ positive electrode currently in use must be replaced with something cheaper. Manganese oxides are potential candidates, but the most common variant based on a spinel structure suffers from a rapid capacity fade at elevated temperatures due to manganese dissolution[1]. Others phases of manganese oxides have also been considered, such as those with tunnel [2] or layered structures [3], [4]. For applications requiring high energy density, layered compounds are the most promising because of the potential for high capacity. However, Bruce *et al.* [5], recently showed that $LiMnO_2$ prepared by ion-exchange of the α-$NaMnO_2$ structure transforms into spinel upon electrochemical cycling. The oxygen arrays in both the O'3 structure of this layered compound and the spinel are cubic close-packed, so that only slight rearrangement of manganese and lithium ions is required for phase conversion to occur. O2 layered lithium manganese oxides, prepared from P2-$Na_{0.7}MnO_{2+z}$, do not have a cubic close-packed oxygen array and do not convert to spinel under normal cycling conditions [6]. Recently, several layered $Li_xM_yMn_{1-y}O_2$ compounds (y=0.1, M=Ni, Co, Al) with O2/O3 intergrowth structures have been prepared by ion exchanging P2/P3 sodium-containing precursors [7]. These intergrowth structures have better electrochemical characteristics than pure O2 compounds and do not appear to convert to spinel.

For this study, we investigated the synthetic parameters that control the P2/P3 ratios in the sodium-containing precursors, and the effect of differing O2/O3 ratios in the lithiated compounds upon the electrochemical properties. An eventual goal is to design a phase-stable electrode with high energy density, suitable for lithium ion batteries.

Experimental

Glycine-nitrate combustion synthesis was used to produced the precursor $Na_xM_yMn_{1-y}O_2$ ($0.5<x<0.7$, $y<0.3$) compounds, as described previously [8]. The desired proportions of $NaNO_3$, 47.5% $Mn(NO_3)_2$ in HNO_3 and substituent metal-nitrate ($Ni(NO_3)_2.9H_2O$, $Co(NO_3)_2.6H_2O$ and $Al(NO_3)_3.9H_2O$) were mixed with glycine in the molar ratio 1:2 and diluted with de-ionized

water. The mixture was heated until combustion occurred and the resultant powder was calcined at 800°C for 4h to remove any organic residue and to ensure homogeneity.

For ion exchange, the materials were refluxed in a solution of LiBr in ethanol (9 fold excess of Li) for 2 days at 80°C. All materials were carefully washed in ethanol to remove any trace of salts and dried at least for 1 day at 150°C.

Elemental compositions were determined by inductively coupled plasma (ICP) analyses (Desert Analytics Laboratory, Tucson, AZ). Powder X-Ray diffraction profiles were recorded by using monochromatized Cu Kα radiation and a Siemens D5000 diffractometer. Powdercell 2.4 for Windows by W. Kraus & G. Nolze was used to quantify the different phases present in the intergrowths and calculate the theoretical patterns shown in the Figures.

Electrodes were prepared as previously described, [8] and assembled into 2032 size coin cells with lithium anodes, Celgard 3401 separators and a 1M $LiPF_6$ electrolyte solution (1:2 (by weight) ethylene carbonate/dimethyl carbonate). Cells were galvanostatically cycled between 4.5V and 2V at a current density of 0.05 $mA.cm^{-2}$ (~ C/50) with a relaxation time of 15 minutes between each half cycle.

Results and discussion

Synthesis and characterization:

We chose the $Na_xNi_{0.2}Mn_{0.8}O_2$ system to demonstrate the effect of the Na:transition metal (Na/TM) ratio upon the relative amounts of P2 and P3 components in intergrowth structures. XRD patterns obtained for three different Na/TM ratios used in the glycine-nitrate combustion are shown in Figure 1. We also show the calculated pattern of the P2 phase $Na_{0.66}Ni_{0.3}Mn_{0.7}O_2$ from Dahn's data [9] and the P3 calculated pattern reported recently by Bruce *et al.*[10]. These results clearly demonstrate that a small change in the Na/TM ratio can drastically modify the intergrowth structure. A pure crystalline P3 compound is obtained at the lowest Na/TM ratio used. At higher sodium contents, structures with increased P2 content are produced. However, pure P2 crystalline powders could not be obtained even by increasing the Na/TM ratio up to 0.8. A rough estimate of the relative proportions of P2 and P3 components can be made from the x-ray powder diffraction data, although satisfactory Rietveld refinements of intergrowth patterns

are difficult to obtain [7]. These values are reported in Table 1, along with the elemental analyses. Note that the sodium contents of the final products are always less than that used for the combustion, indicating loss of sodium during synthesis. The same experiments were carried out using Co as substituting metal ($Na_xCo_yMn_{1-y}O_{2+z}$, $y<0.2$) and a similar influence of the initial Na/TM ratio on relative P2 and P3 contents was observed. For the aluminium substituted compounds, $Na_xAl_yMn_{1-y}O_{2+z}$ ($y=0.11$, 0.15), a $NaAlO_2$ impurity was observed at higher Na/TM ratios [11] complicating the results, and intergrowths, rather than pure P2 or P3 phases, were always obtained.

XRD patterns of ion-exchanged products are given in Figure 2 and show that the P2/P3 intergrowths have been converted into O2/O3 intergrowths. The broadness of the peaks is a consequence of the stacking faults, and, in some cases, may be due to residual sodium, which causes local retention of P-type layers. In some of the patterns, peaks that can be assigned to a separate sodium-containing phase are still apparent, and are more prominent in the materials made from precursors with higher P2 contents. The elemental analyses (Table 2) indicate that P2 compounds are less fully exchanged than P3 ones, resulting in higher residual sodium contents in the lithiated products. In Table 2, we also list designations based upon O2 content (INT0, INT20, INT80), which will be used to refer to these compounds from this point on.

Electrochemical properties:

Cells containing INT0, INT20, and INT80 electrodes are in the partially discharged state and can either be charged or discharged initially. For this study, cells were initially charged and a correlation between structure and initial charge capacity was observed. Although the lithium content increases for materials as the O2/O3 ratio increases, the initial charge capacity decreases, indicating that less lithium can be extracted from the O2 structure. The potential drop during the 15 minutes of relaxation occurring after each oxidation and reduction (for the same current density) is also larger in materials with high O2 content. This is evident in Figure 3, which shows the first discharge curves for the $Li_xNi_{0.2}Mn_{0.8}O_2$ samples after the initial partial charge and 15 minute relaxation step. For all intergrowths, regardless of the substituent, discharge capacities increase as O3 content increases; in this example, INT0 gives 205 mAh/g, INT20, 175 mAh/g, and INT80 145 mAh/g. These results suggest that O2 compounds are somewhat kinetically

limited compared to O3 ones, leading to lower utilization and poorer rate capability. In order to better understand this limitation, experiments using the galvanostatic intermittent titration technique (GITT) and the potential intermittent titration technique (PITT) are presently underway in our laboratory. For INT0 and INT20 electrodes, the capacity at about 4.1 V is most likely due to redox processes of the Ni ion. This is less evident in the INT80 electrode with low O3 content, because of the kinetic limitations associated with extraction of Li ions.

Figure 4 shows discharge curves for the three different samples as a function of the cycle number. All the samples show a significant capacity fade upon cycling between 2.0 and 4.5 V, but the rate of conversion to spinel varies considerably with O3 content. For INT0, the two-plateau profile typical of manganese oxide spinels is quite apparent after 25 cycles. INT20 shows a voltage profile intermediate between that of spinel and layered structures after the same number of cycles, suggesting that conversion is slower. The voltage profile of INT80 has changed only somewhat after 55 cycles. We attribute the greater resistance to phase conversion to the presence of a large amount of O2 component in INT80, since O2 and some O2/O3 intergrowth phases do not rearrange to spinel under normal cycling conditions [6, 7]. Further investigation of the effect of structure on phase conversion using ^{7}Li-MAS NMR and *in situ* XRD is underway in this laboratory.

Conclusions

Layered intergrowth substituted lithiated manganese oxides with different O2/O3 ratio structures were prepared by adjusting the initial Na/TM ratio during synthesis of the sodium-containing precursors. A pure O3 phase was obtained from a low sodium content precursor with a P3 structure has a capacity of 205 mAh/g in lithium cells, when an intergrowth compound containing 80% O2 structure yields only 145 mAh/g, but appears to be more resistant to spinel conversion upon cell cycling. We are currently investigating the possibility of designing electrodes with the phase stability of pure O2 compounds and the high capacity of the O3 structures, by manipulating intergrowth structures.

Acknowledgments

This work was supported by the Assistant Secretary for Energy Efficiency and Renewable Energy, Office of FreedomCAR and Vehicle Technologies of the U.S. Department of Energy under Contract No. DE-AC03-76SF00098.

References

1. Blyr A., Sigala C., Amatucci G., Guyomard D., Chabre Y., Tarascon J-M., *J. Electrochem. Soc.*, **145**, 194 (1998)

2. M. M. Doeff, A. Anapolsky, L. Edman, T. J. Richardson, and L. C. De Jonghe, *J. Electrochem. Soc.*, **148**, A230 (2001).

3. A. R. Armstrong, P. G. Bruce, *Nature,* **381**, 499 (1996).

4. M. M. Thackeray, *Prog. Solid State Chem.,* **25**, 1 (1997).

5. A.D. Robertson, A.R Armstrong and P.G Bruce., *Chem. Mater.*, **13**, 2380 (2001).

6. Z. Lu, R.A Donaberger, C.L Thomas and J.R. Dahn, *J. Electrochem. Soc*, **149**, A1083 (2002).

7. T. A. Eriksson, Y. J. Lee, J. Hollingsworth, J. A. Reimer, E. J. Cairns, X.-F. Zhang, and M. M. Doeff, *Chem. Mater.*, submitted 2003.

8. T. A. Eriksson and M. M. Doeff, *J. Power Sources,* **119-120C**, 145 (2003).

9. J. M. Paulsen and J. R. Dahn, *Solid State Ionics,* **126**, 3 (1999).

10. A. R. Armstrong, A. J. Paterson, A. D. Robertson, P. G. Bruce, *Chem. Mater.*, **14**, 710 (2002).

11. Marca M. Doeff, Joel Hollingsworth, and Mickael Dollé, to be presented at the 204th meeting of the Electrochemical Society, Orlando, FL Oct. 2003.

Table I: Compositions of $Na_xNi_yMn_{1-y}O_{2+z}$ ($y \approx 0.2$) precursors

Initial Na/TM ratio[a]	% P2	% P3	Chemical analysis
0.7	0	100	$Na_{0.49}Ni_{0.18}Mn_{0.82}O_{2+z}$
0.75	20	80	$Na_{0.59}Ni_{0.19}Mn_{0.81}O_{2+z}$
0.8	80	20	$Na_{0.62}Ni_{0.19}Mn_{0.81}O_{2+z}$

a) used in synthesis

Table II : Compositions of $Li_xNi_yMn_{1-y}O_{2+z}$ compounds

Initial Na/TM ratio[a]	Designation	% O2	Chemical analysis
0.7	INT0	0	$Li_{0.64}Na_{0.01}Ni_{0.18}Mn_{0.82}O_{2+z}$
0.75	INT20	20	$Li_{0.65}Na_{0.02}Ni_{0.19}Mn_{0.81}O_{2+z}$
0.8	INT80	80	$Li_{0.73}Na_{0.05}Ni_{0.20}Mn_{0.80}O_{2+z}$

a) used in synthesis of sodium-containing precursors

Figure captions:

Figure 1: XRD patterns of $Na_xNi_{0.2}Mn_{0.8}O_{2+z}$ samples as a function of the Na/TM ratio used in synthesis, and calculated patterns of P2 $Na_{0.66}Ni_{0.3}Mn_{0.7}O_2$ and P3 $Na_{0.5}Ni_{0.33}Mn_{0.67}O_2$. Peaks marked with an asterisk belong to a hydrated P2 phase.

Figure 2: XRD patterns of ion-exchanged compounds obtained from Na-precursors with different initial Na/TM ratios, and calculated patterns of O2 Li_xMnO_{2+z} and O3 Li_xMnO_2. Peaks marked with an asterisk correspond to sodium-containing phases.

Figure 3: First discharges at 0.05 mA/cm^2 of Li/1M $LiPF_6$ EC-DMC/$Li_xNi_{0.2}Mn_{0.8}O_{2+z}$ cells between 2.0 and 4.5 V.

Figure 4: Discharge profiles of Li/1M $LiPF_6$ EC-DMC/$Li_xNi_{0.2}Mn_{0.8}O_{2+z}$ cells at 0.05 mA/cm^2 between 2.0 and 4.5 V for: a) INT0, b) INT20 and c) INT 80. Cycle numbers are indicated on the graphs.

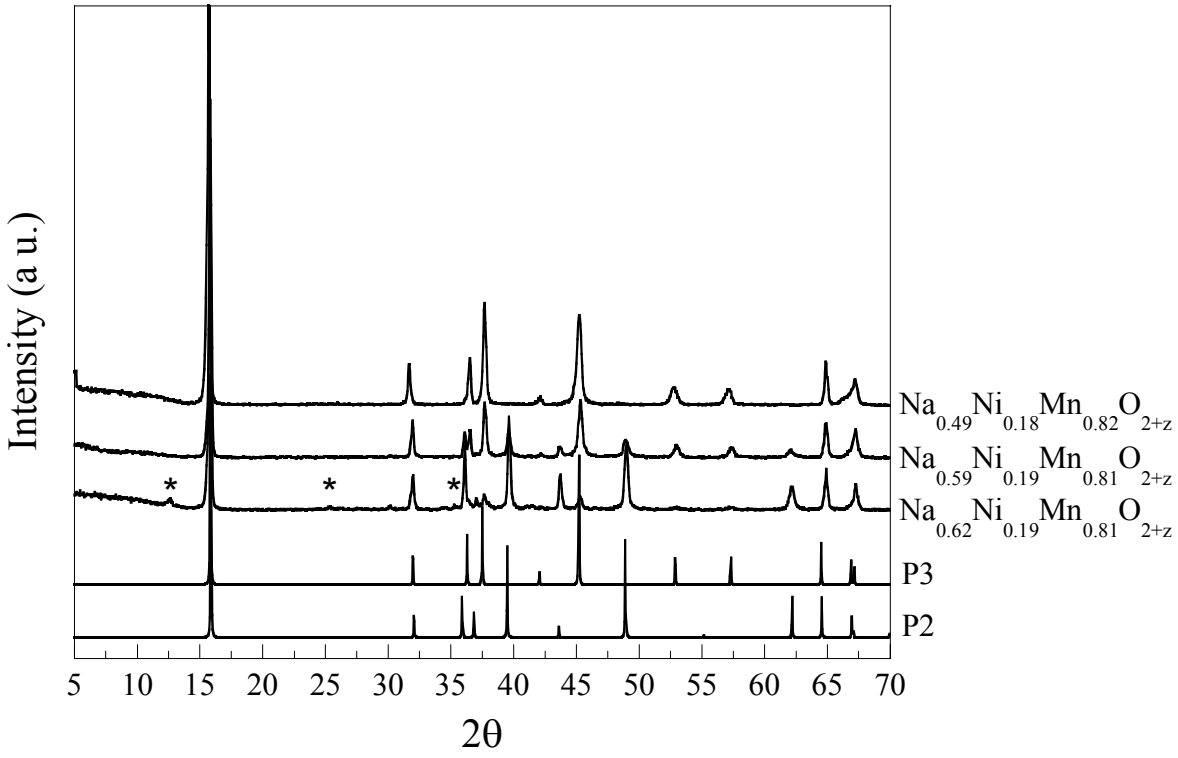
Intensity (a u.)
Na0.49Ni0.18Mn0.82O2+z
Na0.59Ni0.19Mn0.81O2+z
Na0.62Ni0.19Mn0.81O2+z
P3
P2
*
*
*
5 10 15 20 25 30 35 40 45 50 55 60 65 70
2θ

Figure 1

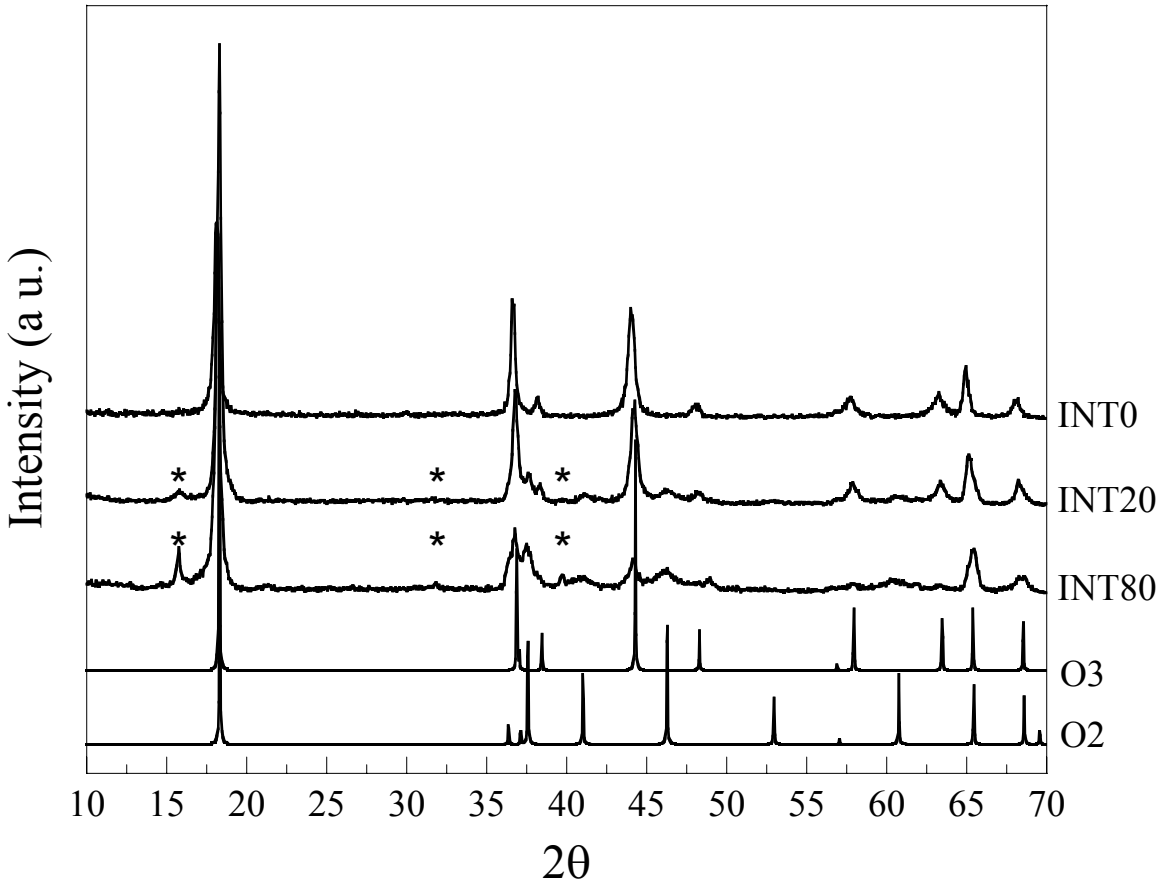
Intensity (a u.)
INT0
INT20
INT80
O3
O2
*
10
15
20
25
30
35
40
45
50
55
60
65
70
2θ

Figure 2

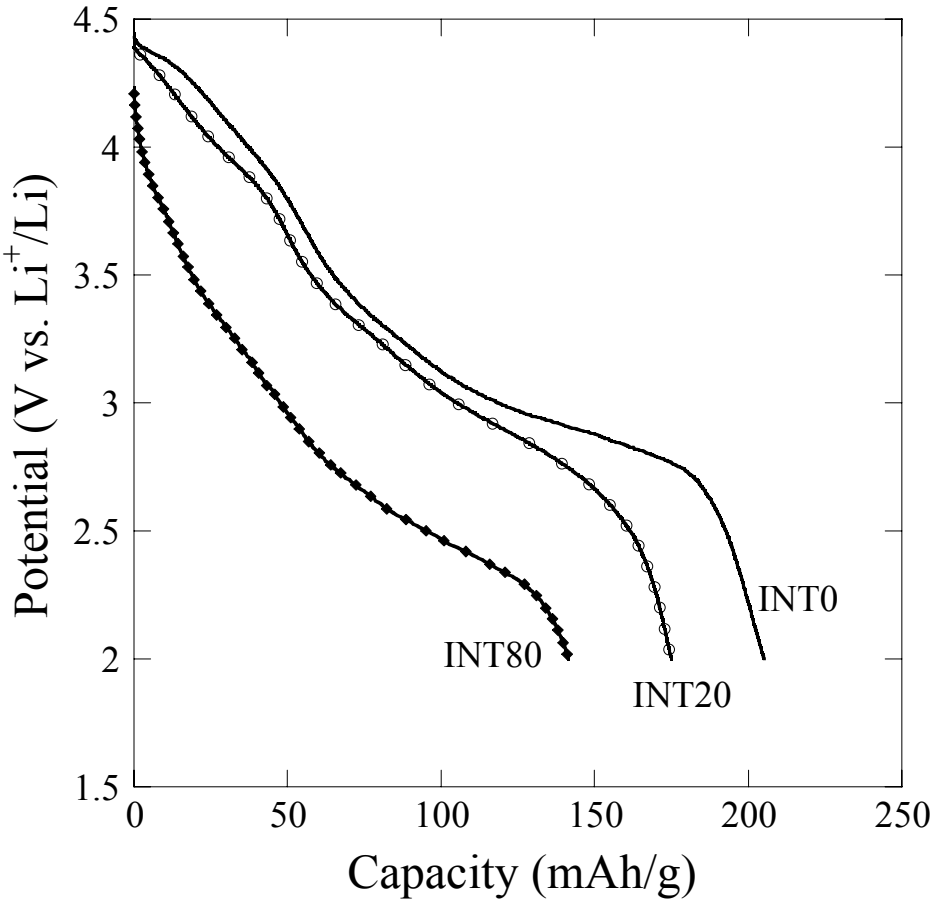
4.5
4
3.5
3
2.5
2
1.5
0
50
100
150
200
250
Potential (V vs. Li+/Li)
Capacity (mAh/g)
INT0
INT20
INT80

Figure 3

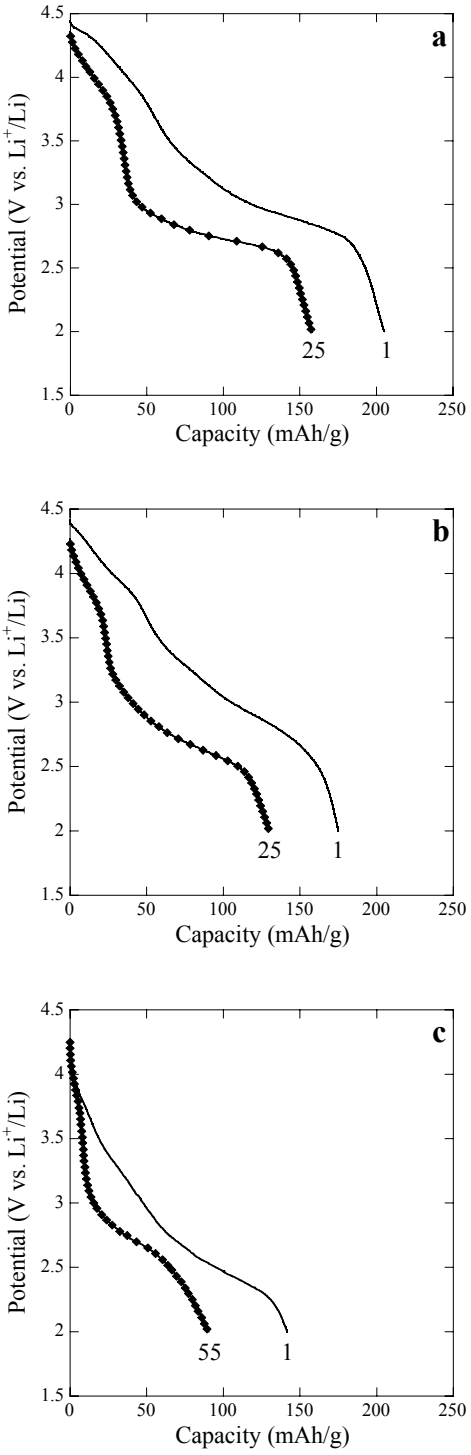
a
b
c
Potential (V vs. Li+/Li)
Capacity (mAh/g)
4.5
4
3.5
3
2.5
2
1.5
0
50
100
150
200
250
25
1
55

Figure 4